ACS NANO

www.acsnano.org

ARTICLE

Liquid-Gated High Mobility and Quantum Oscillation of the Two-Dimensional Electron Gas at an Oxide Interface

Shengwei Zeng,[†,‡] Weiming Lü,[†,■] Zhen Huang,[†] Zhiqi Liu,[†,▲] Kun Han,[†,‡] Kalon Gopinadhan,[†] Changjian Li,[†,§] Rui Guo,[†,#] Wenxiong Zhou,[†,‡] Haijiao Harsan Ma,[†,‡] Linke Jian,[†] Thirumalai Venkatesan,*[,†,‡,§,#,□] and Ariando*[,†,‡,§]

[†]NUSNNI-NanoCore, National University of Singapore, Singapore 117411, Singapore

[‡]Department of Physics, National University of Singapore, Singapore 117542, Singapore

[§]National University of Singapore Graduate School for Integrative Sciences and Engineering (NGS), 28 Medical Drive, Singapore 117456, Singapore

[#]Department of Materials Science and Engineering, National University of Singapore, Singapore 117575, Singapore

[□]Department of Electrical and Computer Engineering, National University of Singapore, Singapore 117576, Singapore

Supporting Information

ABSTRACT: **Electric field effect in electronic double layer transistor (EDLT) configuration with ionic liquids as the dielectric materials is a powerful means of exploring various properties in different materials. Here, we demonstrate the modulation of electrical transport properties and extremely high mobility of two-dimensional electron gas at $LaAlO_3$/$SrTiO_3$ (LAO/STO) interface through ionic liquid-assisted electric field effect. With a change of the gate voltages, the depletion of charge carrier and the resultant enhancement of electron mobility up to 19 380 $cm^2/(V\ s)$ are realized, leading to quantum oscillations of the conductivity at the LAO/STO interface. The present results suggest that high-mobility oxide interfaces, which exhibit quantum phenomena, could be obtained by ionic liquid-assisted field effect.**

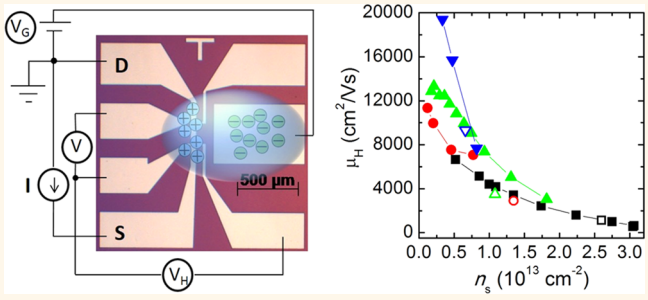

KEYWORDS: *mobility, $LaAlO_3/SrTiO_3$ interfaces, electronic double layer transistors (EDLT), Ionic liquid, electric field effect, Shubnikov–de Haas (SdH) oscillation*

Electric field effect doping has been a flexible and powerful technique to tune the carrier density and the resultant transport properties of a material.[1] More recently, the field effect in EDLT configuration with ionic liquids (ILs) and polymer electrolytes as gate dielectrics has attracted growing interest. In an EDLT, IL is applied directly on the surface of interest and polarized by gate voltage, inducing a two-dimensional (2D) layer of charges on the sample surface with high carrier density of up to $10^{15}/cm^2$.[2] Owing to the capability of EDLTs in accumulating large amount of carriers, electric field-induced phase transitions have been demonstrated in various materials.[2−7] In the push for practical application of ILs-assisted field-effect transistors, it is desirable to obtain high carrier mobility at the 2D layer. However, since the ILs are applied on the sample surface, disorder is induced due to surface-degrading electrochemical reactions,[7−9] which hinders the improvement of the mobility. For example, the reported mobility is ~1000 $cm^2/(V\ s)$ at IL/$SrTiO_3$,[3] ~250 $cm^2/(V\ s)$ at IL/ZnO,[2] ~7000 $cm^2/(V\ s)$ at IL/$KTaO_3$ interfaces below 10 K,[4] and ~330 $cm^2/(V\ s)$ at interfaces between IL and 2D materials at 77 K.[10−13] Therefore, protection of surface would help to improve the mobility of the induced 2D charged layer.[14] For the 2D electron gas (2DEG) at the interface between two insulators formed by depositing thin film on substrate, it is expected that the mobility can be improved by IL gating since the deposited capping layer can be used as the protection layer. Here, we demonstrate a high-mobility 2DEG at LAO/STO interface as a result of IL gating.

Among oxide interfaces, LAO/STO interface is of particular interest since it exhibited fascinating properties such as conductivity,[15] superconductivity,[16] magnetism,[17] electronic phase separation,[18] 2D quantum oscillations,[19−22] and con-

Received: January 18, 2016
Accepted: March 9, 2016
Published: March 9, 2016

DOI: 10.1021/acsnano.6b00409
ACS Nano 2016, 10, 4532−4537

troversial origin of conductivity.[23] These phenomena provide new insights for understanding the nature of electronic and magnetic properties at strongly correlated oxide interfaces. Enhancements of mobility at LAO/STO interfaces and STO-based heterostructures have been explored through defect engineering,[24] surface control,[25] dimensionality control,[26] charge-transfer-induced modulation doping,[27] and growth strategies.[19,28−31] Electric field effect could modulate charge carriers and be flexibly implemented on devices; it is therefore vital to explore its tunability of the LAO/STO interfaces. Electric field induced insulator-to-metal and superconductor-to-insulator transitions have been demonstrated using STO,[32−34] LAO,[35−39] ferroelectric $Pb(Zr_{0.2}Ti_{0.8})O_3$,[40,41] Si_3N_4,[42] and IL[43] as the dielectric materials. However, to the best of our knowledge, there is no report on significant enhancement of mobility at the LAO/STO interface by means of electric field effect; only a slight enhancement (from ∼1000 to ∼2000 $cm^2/(V\ s)$) or even reduction in mobility was observed.[34,35,38] In this paper, we demonstrate the modulation of electrical transport properties of LAO/STO interface by electric field effect in EDLT configuration. Through changing the gate voltage, the carrier density at the interface is depleted, and therefore, the mobility is significantly enhanced up to 19 380 $cm^2/(V\ s)$ at low temperature. Due to enhancement of mobility, clear quantum oscillations of the conductance is observed.

RESULTS AND DISCUSSION

Figure 1a shows an optical micrograph of a typical pattern on STO for field effect measurement. The width of the Hall bar is 50 μm (some of devices have width of 200 μm) and length is 500 μm; the distance between two voltage probes is 160 μm. A six-probe configuration of the Hall bar allows for the measurement of both longitudinal and Hall resistance. Figure 1b shows an atomic force microscopy (AFM) image of 10-uc LAO grown on the patterned STO substrate. Clear atomic terraces are observed, indicating the smooth surface of patterned substrate and high-quality thin films. Figure 1c,d shows source-drain current (I_D), leakage current (I_G), and resistance as a function of gate voltage (V_G). It can be seen that I_G is within 1 nA and independent of V_G. This negligibly small I_G indicates a good operation of the device. I_D is significantly higher than I_G at high V_G, and decreases with decreasing V_G down to the value of I_G at $V_G \approx -0.6$ V. Resistance increases with decreasing V_G up to the measurement limit at $V_G \approx -0.6$ V. The V_G needed to obtain the insulating state is significantly lower than that in back-gating device (which is on the order of 100 V).[32−34] When the V_G is scanned between −0.8 and 2 V, reversible metal−insulator transition with an ON/OFF ratio of $\sim 10^4$ is observed and the transition is nonhysteretic, which can be seen from the fact that the curves of three scan cycles are significantly similar.

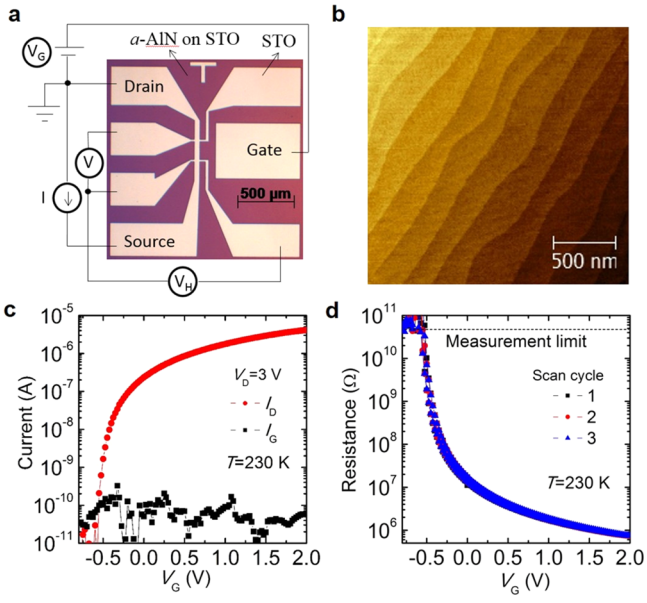

Figure 1. Optical micrograph, surface and electrical transport characterization of an LAO/STO EDLT. (a) Optical micrograph of a Hall-bar pattern on STO using amorphous AlN as the mask and the measurement circuit. (b) AFM image for 10 uc LAO grown on patterned STO substrates, measured in the region of Hall bar channel. (c) Source-drain current I_D and leakage current I_G as a function of gate voltages V_G. (d) Resistance as a function of V_G for a device for three scan cycles. Each scan cycle starts from 0 to 2 V, and then from 2 to −0.8 V, and finally from −0.8 to 0 V. The scan speed of V_G is 25 mV/s.

To fully demonstrate the validity of mobility enhancement by IL gating, four samples (samples A−D) with different initial low-temperature mobilities were synthesized and characterized (see Methods). Figure 2a shows the sheet resistance *versus* temperature (R_s-T) curves at various V_G for sample A. The R_s-T curves for samples B−D are shown in Supporting Information Figure S2. Before the R_s-T curves measurements, the V_G was applied at 230 K and kept for 10 min for charging. Resistance measurement was made as the samples were cooled down while keeping the V_G constant. To change V_G, the sample was heated to 230 K after each R_s-T curve measurement and a new V_G was applied. At $-0.4 \le V_G \le 3$ V, the sample exhibits metallic behavior, showing a decrease in R_s as T is reduced. At high T, as the V_G is increased, R_s decreases monotonously (Figure 2a). This indicates that increasing V_G causes enhancement of carrier density at the interface. However, at low T, R_s does not show monotonous change with increasing V_G. R_s decreases as V_G is increased from −0.4 to 0 V, while it increases

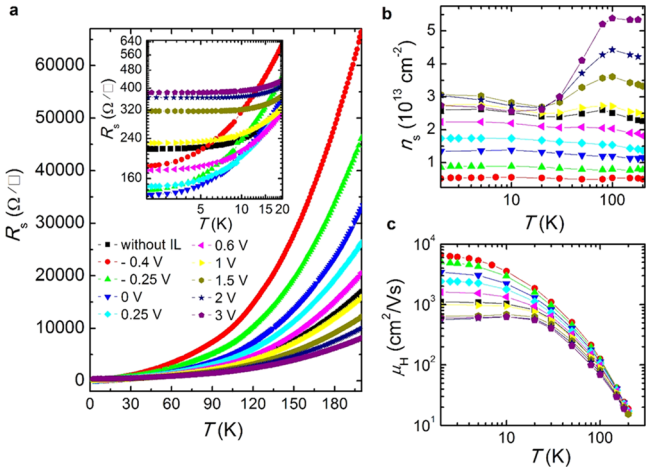

Figure 2. Electrical transport characterization of an LAO/STO EDLT. (a) The linear-scale sheet resistance *versus* temperature (R_s-T) curves at various V_G for sample A. Inset of (a) is the logarithmic-scale R_s-T curves at low temperature. (b) The n_s and (c) μ_H as a function of temperature at various V_G for sample A. The black square is the data without IL on top of the sample.

DOI: 10.1021/acsnano.6b00409
ACS Nano 2016, 10, 4532−4537

as V_G is increased from 0 to 3 V (inset of Figure 2a). At $V_G \geq$ 1.5 V, R_s shows a slight upturn at T below ~5 K, suggesting localization at high V_G. However, at -0.4 V $\leq V_G \leq$ 1 V, the sample shows completely metallic behavior down to 2 K, suggesting that charge carriers are less scattered at this V_G regime.

The carrier density n_s as a function of T at various V_G for sample A is shown in Figure 2b. At high T regime, n_s increases with increasing V_G. However, at low T regime from 20 to 2 K, n_s increases with increasing V_G from -0.4 to 1 V and saturates at ~3×10^{13} cm^{-2} for $V_G \geq$ 1.5 V. The saturation of n_s at 2 K can be clearly seen in Figure 3a. For the dependence of n_s on T,

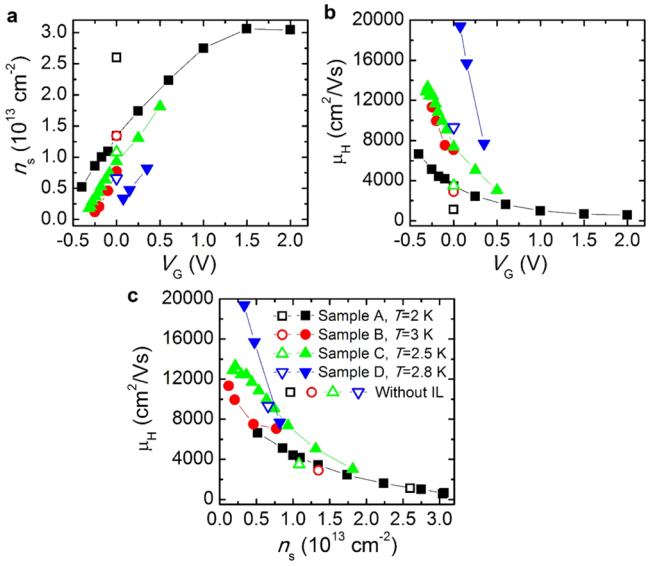

Figure 3. Carrier density n_s and mobility μ_H at low temperature. (a) The n_s and (b) μ_H as a function of V_G for samples A–D at low temperatures. (c) The μ_H as a function of n_s. The data for samples without IL are also shown.

behavior of n_s is different between two V_G regimes. For $V_G \leq$ 1 V, n_s is nearly T-independent at each V_G. For $V_G \geq$ 1.5 V, n_s generally decreases with decreasing T, suggesting the carrier freeze-out effect. In contrast to n_s, Hall mobility μ_H increases with decreasing T at all V_G values, as shown in Figure 2c. For example, at $V_G = -0.4$ V, μ_H increases from ~24 cm^2/(V s) at 180 K to ~6600 cm^2/(V s) at 2 K. For the dependence of μ_H on V_G, at high T of 180 K, μ_H exhibits little V_G dependence, changing from 20 cm^2/(V s) at V_G = 2 V to 24 cm^2/(V s) at $V_G = -0.4$ V. However, at low T, a significant change of μ_H is observed. For example, at T = 2 K, μ_H increases from ~650 cm^2/(V s) at V_G = 2 V to ~6600 cm^2/(V s) at $V_G = -0.4$ V (see also Figure 3a).

The R_s–T, n_s–T, and μ_H–T curves for the sample A without IL on top of LAO are also plotted in Figure 2. One can see that the curves for the sample without IL and for the sample with IL but without application of V_G (V_G = 0 V) do not coincide with each other. The sample with V_G = 0 V show higher R_s at high T but lower R_s at low T, compared with that for sample without IL. Moreover, at V_G = 0 V, the n_s is lower and μ_H is higher than that without IL. These suggest that there is a coupling between the interface and surface which was covered by IL even at V_G = 0 V, causing depletion of n_s at the interface. The interface–surface coupling and the resultant change of electrical transport properties of LAO/STO heterostructures have also been observed by capping polar chemical solvents such as acetone, ethanol, and water on top of LAO surface.[25,44,45] Enhancements of n_s and reduction of μ_H were obtained by covering the polar solvents.[44] However, our results show the opposite behavior with reduction of n_s and enhancement of μ_H. This may be due to the different properties between polar solvents and IL.

Figure 3 shows the n_s and μ_H as a function of V_G and μ_H as a function of n_s at low T for four samples with different initial n_s and μ_H. One can see that for all samples, significant depletion of n_s and enhancement of μ_H are obtained by increasing negative V_G. Considering that $\mu_H = 1/(e \cdot n_s \cdot R_s)$, where e is the elementary charge, and that R_s does not change much with V_G at low T (Figure 2a and Supporting Information Figure S2), we are able to attribute enhancement of μ_H to the depletion of n_s. This can be clearly seen in Figure 3c, showing that μ_H increases with decreasing n_s over a broad n_s range. The highest mobilities obtained here are 6600 cm^2/(V s) at 5×10^{12} cm^{-2}, 11 330 cm^2/(V s) at 1.2×10^{12} cm^{-2}, 13 320 cm^2/(V s) at 2.1×10^{12} cm^{-2}, and 19 380 cm^2/(V s) at 3.3×10^{12} cm^{-2} for samples A, B, C, and D, respectively, which are significantly higher than those before IL gating, 1110, 2900, 3500, and 9300 cm^2/(V s) for samples A, B, C, and D, respectively. The data without IL are also plotted in Figure 3. As discussed above, due to the interface–surface coupling, depletion of n_s and enhancement of μ_H after covering IL are observed. Compared with the ones without IL, after covering IL (V_G = 0 V), μ_H increases from 1110 to 3400 cm^2/(V s), from 2900 to 7060 cm^2/(V s), and from 3500 to 7360 cm^2/(V s) for samples A, B, and C, respectively. For sample D, after covering IL, it shows highly insulating at low T and the resistance is out of the measurement limit at V_G = 0 V. This may be because sample D has lower initial n_s (6.6×10^{12} cm^{-2}), leading to a much lower n_s as the IL is applied on the surface of the sample, which could not support the metallic behavior. Upon increasing the V_G and therefore increasing n_s, sample D shows metallic behavior and highest mobility of 19 380 cm^2/(V s) at T = 2.8 K for V_G = 0.075 V.

It has been shown that IL gating causes degradation of the sample surface due to the electrochemical reaction.[7–9,46] However, the AFM images of the sample surfaces before and after gating experiments show that the surfaces are significantly similar (Supporting Information Figure S3). Moreover, the IL-gated metal–insulator transition is reversible and nonhysteretic, and the leakage current is significantly small (Figure 1c,d). These results suggest that the interfaces do not degrade after IL gating, and therefore, significant enhancement of mobility could be obtained. The enhancement of mobility in the present result is more obvious than that in conventional gating using STO (from ~2400 to ~3600 cm^2/(V s)) and LAO (from ~1000 to ~2000 cm^2/(V s)) as the dielectric material.[19,34,35] The highest mobility is much higher than that in the EDLTs without protection layer (*e.g.*, ~1000 cm^2/(V s) at IL/STO interface and ~7000 cm^2/(V s) at IL/$KTaO_3$ interface),[2–4,10–13] and that in the EDLT on STO using BN as a protection layer (12 000 cm^2/(V s)).[14]

To further demonstrate the enhancement of mobility by IL-assisted field effect, we show the observation of the Shubnikov–de Haas (SdH) oscillation in the magneto-resistance (MR) measurement. Figure 4a shows the variation of resistance $\Delta R = R(B) - R(0)$ at different V_G as a function of magnetic field B oriented perpendicular to the LAO/STO interface, measured at T = 2 K for sample A. For the sample without IL, positive MR and no oscillation are observed for B

DOI: 10.1021/acsnano.6b00409
ACS Nano 2016, 10, 4532–4537

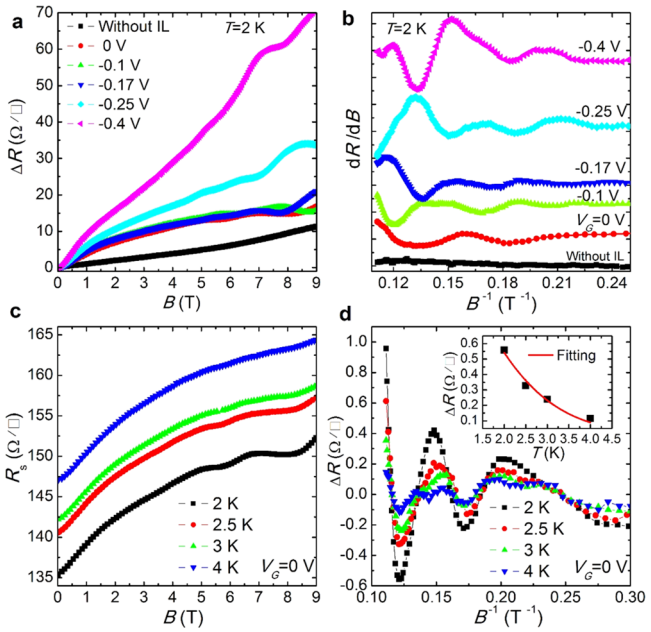

Figure 4. Liquid-gated modulation of the Shubnikov–de Haas oscillations for sample A. (a) Variation of resistance $\Delta R = R(B) - R(0)$ as a function of magnetic field B. (b) Numerical derivative dR/dB as a function of the inverse of magnetic field B^{-1}. (c) Sheet resistance as a function of B for different temperatures at $V_G = 0$ V. (d) Oscillatory component of the sheet resistance as a function of B^{-1}. Inset of (d) is the amplitude of the oscillation at $B = 8.25$ T as a function of temperature. The black squares are the experimental data and the red curve is the fitting line.

up to 9 T. After application of IL, ΔR oscillation is observed for B higher than ~4 T even at $V_G = 0$ V, due to the enhancement of mobility (Figure 3). ΔR oscillation is also observed at higher negative V_G for $-0.4\ \text{V} \le V_G \le 0$ V. Figure 4b shows numerical derivative of resistance dR/dB as a function of the inverse of magnetic field B^{-1}. One can see that the oscillations are more visible in dR/dB *versus* B^{-1} plots and the oscillations are periodic in B^{-1} at each V_G. With increasing negative V_G and thereby decreasing n_s, the significant shift of the main peak of the oscillations is observed.

Figure 4c shows the R_s as a function of B for different T at $V_G = 0$ V. When a polynomial background is subtracted for each curve, the amplitude of oscillation is obtained and shown in Figure 4d. One can see that the amplitude decreases with increasing T. The oscillation amplitude ΔR as a function of T can be described by the relation[19,20]

$$\Delta R(T) = 4R_0 e^{-\alpha T_D} \alpha T / \sinh(\alpha T) \quad (1)$$

where $\alpha = 2\pi^2 k_B/\hbar\omega_c$, $\omega_c = eB/m^*$, k_B is the Boltzmann constant, $\hbar$ is the Planck constant, ω_c is the cyclotron frequency, e is the elementary charge, B is the magnetic field, m^* is the carrier effective mass, R_0 is the nonoscillatory component of R_s, and T_D is the Dingle temperature. We extracted ΔR at $B = 8.25$ T (the peak at $B^{-1} = 0.121\ \text{T}^{-1}$) and plotted it as a function of T in the inset of Figure 4d. The fitting of these data by using the equation (eq 1) gives the effective mass $m^* = 0.70 \pm 0.06\ m_e$, where m_e is free electron mass. The value of m^* observed here is lower than that of previous high-mobility LAO/STO interfaces,[19−22] and is comparable to that of LAO/STO interface treated by surface control.[22]

CONCLUSION

In summary, we have performed the IL-assisted electric field effect to tune the transport properties of 2DEG at LAO/STO interface. Depletion of carrier density and the resultant metal–insulator transitions are observed. The LAO capping layer separates the IL from the 2DEG, and therefore, the interface is protected against any electrochemical reaction, which is suggested by facts that the sample surfaces before and after IL gating are unchanged and the metal–insulator transitions are reversible. Therefore, the mobility was significantly enhanced as the carrier density is depleted. Due to the mobility enhancement, SdH oscillations of the conductance were observed. These results suggest that ionic liquid-assisted field effect could be an important avenue to construct high-mobility oxide interfaces which are essential for exploration of quantum phenomena. Moreover, the samples show a significant response on the electric field and exhibit a reversible metal–insulator transition with high ON/OFF ratios, which are potential for device applications such as field effect transistors and electronic switches.

METHODS

The LAO/STO heterostructures were obtained by depositing LAO thin films on TiO_2-terminated (100)-oriented STO substrates using pulsed laser deposition (PLD) system. The target is single crystalline LAO. Four samples (samples A–D) with different initial low-T mobilities were synthesized. Sample A was deposited at temperature T = 760 °C and has initial mobility of 1110 $cm^2/(V\ s)$ at T = 2 K. Samples B, C, and D were deposited at T = 650 °C and have initial mobilities of 2900 $cm^2/(V\ s)$ at T = 3 K, 3500 $cm^2/(V\ s)$ at T = 2.5 K, and 9300 $cm^2/(V\ s)$ at T = 2.8 K, respectively. The enhanced initial mobilities for sample B, C, and D are attributed to the improvement of crystalline quality of LAO deposited at low T. The thickness of samples A, B, C, and D is 10, 8, 8, and 8 unit cells (uc), respectively. Sample A was deposited at oxygen partial pressure $P_{O2} = 2 \times 10^{-3}$ Torr, and samples B–D were deposited at $P_{O2} = 2 \times 10^{-4}$ Torr, and then they all were cooled down to room temperature in the deposition P_{O2} at a rate of 15 °C/min. During the deposition, an *in situ* reflection high energy electron diffraction (RHEED) was used to monitor the thickness of LAO (Supporting Information Figure S1). Patterns with a Hall bar geometry and a lateral gate electrode were fabricated to form IL-assisted field-effect devices. To fabricate patterned LAO/STO interfaces, before the deposition of LAO, STO substrates were patterned by using conventional photolithography, and amorphous AlN films were deposited as a hard mask. Then, the patterned substrates were put into PLD chamber for the deposition of LAO. After deposition, the samples were annealed in a tube furnace at 550 °C for 1 h in air, in order to remove the oxygen vacancies in STO introduced by high-energy plasma bombardment during the deposition.

After the thin film growth, we did not carry out any processing step such as lithography because exposing the samples to chemicals may deteriorate the quality of surface and interface. The wire connection for transport measurement was done by Al ultrasonic wire bonding. For the connection of gate electrodes, Al wires were first bonded to the lateral gate pads, and then a small amount of silver paint was dropped to cover the gate pad. The silver paint is used to enlarge the area of the gate electrode, enabling the accumulation of ions. A small droplet of an IL, *N*,*N*-diethyl-*N*-methyl-*N*-(2-methoxyethyl)-ammonium bis(trifluoromethyl sulphonyl)imide (DEME-TFSI), was put onto the sample and covered both the conducting channel and the gate electrode. The sample was then placed in the chamber of a Quantum Design Physical Property Measurement System (PPMS) for the transport measurement.

DOI: 10.1021/acsnano.6b00409
ACS Nano 2016, 10, 4532–4537

ASSOCIATED CONTENT

Supporting Information

The Supporting Information is available free of charge on the ACS Publications website at DOI: 10.1021/acsnano.6b00409.

Characterization of sample growth using reflection high energy electron diffraction (RHEED), electrical characterization of samples B–D, and surface characterization of samples before and after gating experiments (PDF)

AUTHOR INFORMATION

Corresponding Authors

*E-mail: venky@nus.edu.sg.

*E-mail: ariando@nus.edu.sg.

Present Addresses

■Department of Science, Condense Matter Science and Technology Institute, Harbin Institute of Technology, Harbin 150001, China.

▲Department of Materials Science and Engineering, University of California, Berkeley, California 94720, USA.

Notes

The authors declare no competing financial interest.

ACKNOWLEDGMENTS

This work is supported by the National University of Singapore (NUS) Academic Research Fund (AcRF Tier 1 Grant No. R-144-000-346-112 and R-144-000-364-112) and the Singapore National Research Foundation (NRF) under the Competitive Research Programs (CRP Award No. NRF-CRP 8-2011-06 and CRP Award No. NRF-CRP10-2012-02).

REFERENCES

(1) Ahn, C. H.; Bhattacharya, A.; Ventra, M. D.; Eckstein, J. N.; Frisbie, C. D.; Gershenson, M. E.; Goldman, A. M.; Inoue, I. H.; Mannhart, J.; Millis, A. J.; Morpurgo, A. F.; Natelson, D.; Triscone, J. M. Electrostatic Modification of Novel Materials. *Rev. Mod. Phys.* **2006**, *78*, 1185–1212.

(2) Yuan, H. T.; Shimotani, H.; Tsukazaki, A.; Ohtomo, A.; Kawasaki, M.; Iwasa, Y. High-Density Carrier Accumulation in ZnO Field-Effect Transistors Gated by Electric Double Layers of Ionic Liquids. *Adv. Funct. Mater.* **2009**, *19*, 1046–1053.

(3) Ueno, K.; Nakamura, S.; Shimotani, H.; Ohtomo, A.; Kimura, N.; Nojima, T.; Aoki, H.; Iwasa, Y.; Kawasaki, M. Electric-Field-Induced Superconductivity in an Insulator. *Nat. Mater.* **2008**, *7*, 855–858.

(4) Ueno, K.; Nakamura, S.; Shimotani, H.; Yuan, H. T.; Kimura, N.; Nojima, T.; Aoki, H.; Iwasa, Y.; Kawasaki, M. Discovery of Superconductivity in $KTaO_3$ by Electrostatic Carrier Doping. *Nat. Nanotechnol.* **2011**, *6*, 408–412.

(5) Ye, J. T.; Zhang, Y. J.; Akashi, R.; Bahramy, M. S.; Arita, R.; Iwasa, Y. Superconducting Dome in a Gate-Tuned Band Insulator. *Science* **2012**, *338*, 1193–1196.

(6) Zeng, S. W.; Huang, Z.; Lv, W. M.; Bao, N. N.; Gopinadhan, K.; Jian, L. K.; Herng, T. S.; Liu, Z. Q.; Zhao, Y. L.; Li, C. J.; Ma, H. J. H.; Yang, P.; Ding, J.; Venkatesan, T.; Ariando. Two-Dimensional Superconductor-Insulator Quantum Phase Transitions in an Electron-Doped Cuprate. *Phys. Rev. B: Condens. Matter Mater. Phys.* **2015**, *92*, 020503.

(7) Jeong, J.; Aetukuri, N.; Graf, T.; Schladt, T. D.; Samant, M. G.; Parkin, S. S. P. Suppression of Metal-Insulator Transition in VO_2 by Electric Field-Induced Oxygen Vacancy Formation. *Science* **2013**, *339*, 1402–1405.

(8) Schladt, T. D.; Graf, T.; Aetukuri, N. B.; Li, M. Y.; Fantini, A.; Jiang, X.; Samant, M. G.; Parkin, S. S. P. Crystal-Facet-Dependent Metallization in Electrolyte-Gated Rutile TiO_2 Single Crystals. *ACS Nano* **2013**, *7*, 8074–8081.

(9) Petach, T. A.; Lee, M.; Davis, R. C.; Mehta, A.; Goldhaber-Gordon, D. Mechanism for the Large Conductance Modulation in Electrolyte-Gated Thin Gold Films. *Phys. Rev. B: Condens. Matter Mater. Phys.* **2014**, *90*, 081108.

(10) Zhang, Y. J.; Ye, J. T.; Matsuhashi, Y.; Iwasa, Y. Ambipolar MoS_2 Thin Flake Transistors. *Nano Lett.* **2012**, *12*, 1136–1140.

(11) Chuang, H. J.; Tan, X. B.; Ghimire, N. J.; Perera, M. M.; Chamlagain, B.; Cheng, M. M. C.; Yan, J. Q.; Mandrus, D.; Tomanek, D.; Zhou, Z. X. High Mobility WSe_2 p- and n-Type Field-Effect Transistors Contacted by Highly Doped Graphene for Low-Resistance Contacts. *Nano Lett.* **2014**, *14*, 3594–3601.

(12) Perera, M. M.; Lin, M. W.; Chuang, H. J.; Chamlagain, B. P.; Wang, C.; Tan, X.; Cheng, M. M. C.; Tomanek, D.; Zhou, Z. Improved Carrier Mobility in Few-Layer MoS_2 Field-Effect Transistors with Ionic-Liquid Gating. *ACS Nano* **2013**, *7*, 4449–4458.

(13) Saito, Y.; Iwasa, Y. Ambipolar Insulator-to-Metal Transition in Black Phosphorus by Ionic-Liquid Gating. *ACS Nano* **2015**, *9*, 3192–3198.

(14) Gallagher, P.; Lee, M.; Petach, T. A.; Stanwyck, S. W.; Williams, J. R.; Watanabe, K.; Taniguchi, T.; Goldhaber-Gordon, D. A High-Mobility Electronic System at an Electrolyte-Gated Oxide Surface. *Nat. Commun.* **2015**, *6*, 6437.

(15) Ohtomo, A.; Hwang, H. Y. A High-Mobility Electron Gas at the $LaAlO_3/SrTiO_3$ Heterointerface. *Nature* **2004**, *427*, 423–426.

(16) Reyren, N.; Thiel, S.; Caviglia, A. D.; Kourkoutis, L. F.; Hammerl, G.; Richter, C.; Schneider, C. W.; Kopp, T.; Ruetschi, A. S.; Jaccard, D.; Gabay, M.; Muller, D. A.; Triscone, J. M.; Mannhart, J. Superconducting Interfaces Between Insulating Oxides. *Science* **2007**, *317*, 1196–1199.

(17) Brinkman, A.; Huijben, M.; Van Zalk, M.; Huijben, J.; Zeitler, U.; Maan, J. C.; Van der Wiel, W. G.; Rijnders, G.; Blank, D. H. A.; Hilgenkamp, H. Magnetic Effects at the Interface Between Non-Magnetic Oxides. *Nat. Mater.* **2007**, *6*, 493.

(18) Ariando; Wang, X.; Baskaran, G.; Liu, Z. Q.; Huijben, J.; Yi, J. B.; Annadi, A.; Barman, A. R.; Rusydi, A.; Dhar, S.; Feng, Y. P.; Ding, J.; Hilgenkamp, H.; Venkatesan, T. Electronic Phase Separation at the $LaAlO_3/SrTiO_3$ Interface. *Nat. Commun.* **2011**, *2*, 188.

(19) Caviglia, A. D.; Gariglio, S.; Cancellieri, C.; Sacepe, B.; Fete, A.; Reyren, N.; Gabay, M.; Morpurgo, A. F.; Triscone, J. M. Two-Dimensional Quantum Oscillations of the Conductance at $LaAlO_3/SrTiO_3$ Interfaces. *Phys. Rev. Lett.* **2010**, *105*, 236802.

(20) Ben Shalom, M.; Ron, A.; Palevski, A.; Dagan, Y. Shubnikov-De Haas Oscillations in $SrTiO_3/LaAlO_3$ Interface. *Phys. Rev. Lett.* **2010**, *105*, 206401.

(21) McCollam, A.; Wenderich, S.; Kruize, M. K.; Guduru, V. K.; Molegraaf, H. J. A.; Huijben, M.; Koster, G.; Blank, D. H. A.; Rijnders, G.; Brinkman, A.; Hilgenkamp, H.; Zeitler, U.; Maan, J. C. Quantum Oscillations and Subband Properties of the Two-Dimensional Electron Gas at the $LaAlO_3/SrTiO_3$ Interface. *APL Mater.* **2014**, *2*, 022102.

(22) Xie, Y.; Bell, C.; Kim, M.; Inoue, H.; Hikita, Y.; Hwang, H. Y. Quantum Longitudinal and Hall Transport at the $LaAlO_3/SrTiO_3$ Interface at Low Electron Densities. *Solid State Commun.* **2014**, *197*, 25–29.

(23) Liu, Z. Q.; Li, C. J.; Lu, W. M.; Huang, X. H.; Huang, Z.; Zeng, S. W.; Qiu, X. P.; Huang, L. S.; Annadi, A.; Chen, J. S.; Coey, J. M. D.; Venkatesan, T.; Ariando. Origin of the Two-Dimensional Electron Gas at $LaAlO_3/SrTiO_3$ Interfaces: The Role of Oxygen Vacancies and Electronic Reconstruction. *Phys. Rev. X* **2013**, *3*, 021010.

(24) Huijben, M.; Koster, G.; Kruize, M. K.; Wenderich, S.; Verbeeck, J.; Bals, S.; Slooten, E.; Shi, B.; Molegraaf, H. J. A.; Kleibeuker, J. E.; van Aert, S.; Goedkoop, J. B.; Brinkman, A.; Blank, D. H. A.; Golden, M. S.; van Tendeloo, G.; Hilgenkamp, H.; Rijnders, G. Defect Engineering in Oxide Heterostructures by Enhanced Oxygen Surface Exchange. *Adv. Funct. Mater.* **2013**, *23*, 5240–5248.

(25) Xie, Y.; Bell, C.; Hikita, Y.; Harashima, S.; Hwang, H. Y. Enhancing Electron Mobility at the $LaAlO_3/SrTiO_3$ Interface by Surface Control. *Adv. Mater.* **2013**, *25*, 4735–4738.

DOI: 10.1021/acsnano.6b00409
ACS Nano 2016, 10, 4532–4537

(26) Irvin, P.; Veazey, J. P.; Cheng, G. L.; Lu, S. C.; Bark, C. W.; Ryu, S.; Eom, C. B.; Levy, J. Anomalous High Mobility in $LaAlO_3/SrTiO_3$ Nanowires. *Nano Lett.* **2013**, *13*, 364−368.
(27) Chen, Y. Z.; Trier, F.; Wijnands, T.; Green, R. J.; Gauquelin, N.; Egoavil, R.; Christensen, D. V.; Koster, G.; Huijben, M.; Bovet, N.; Macke, S.; He, F.; Sutarto, R.; Andersen, N. H.; Sulpizio, J. A.; Honig, M.; Prawiroatmodjo, G. E. D. K.; Jespersen, T. S.; Linderoth, S.; Ilani, S.; et al. Extreme Mobility Enhancement of Two-Dimensional Electron Gases at Oxide Interfaces by Charge-Transfer-Induced Modulation Doping. *Nat. Mater.* **2015**, *14*, 801−806.
(28) Chen, Y. Z.; Bovet, N.; Trier, F.; Christensen, D. V.; Qu, F. M.; Andersen, N. H.; Kasama, T.; Zhang, W.; Giraud, R.; Dufouleur, J.; Jespersen, T. S.; Sun, J. R.; Smith, A.; Nygard, J.; Lu, L.; Buchner, B.; Shen, B. G.; Linderoth, S.; Pryds, N. A High-Mobility Two-Dimensional Electron Gas at the Spinel/Perovskite Interface of Gamma-$Al_2O_3/SrTiO_3$. *Nat. Commun.* **2013**, *4*, 1371.
(29) Son, J.; Moetakef, P.; Jalan, B.; Bierwagen, O.; Wright, N. J.; Engel-Herbert, R.; Stemmer, S. Epitaxial $SrTiO_3$ films with electron mobilities exceeding 30,000 $cm^2 V^{-1}s^{-1}$. *Nat. Mater.* **2010**, *9*, 482−484.
(30) Choi, W. S.; Lee, S.; Cooper, V. R.; Lee, H. N. Fractionally delta-Doped Oxide Superlattices for Higher Carrier Mobilities. *Nano Lett.* **2012**, *12*, 4590−4594.
(31) Fete, A.; Cancellieri, C.; Li, D.; Stornaiuolo, D.; Caviglia, A. D.; Gariglio, S.; Triscone, J. M. Growth-Induced Electron Mobility Enhancement at the $LaAlO_3/SrTiO_3$ Interface. *Appl. Phys. Lett.* **2015**, *106*, 051604.
(32) Thiel, S.; Hammerl, G.; Schmehl, A.; Schneider, C. W.; Mannhart, J. Tunable Quasi-Two-Dimensional Electron Gases in Oxide Heterostructures. *Science* **2006**, *313*, 1942−1945.
(33) Caviglia, A. D.; Gariglio, S.; Reyren, N.; Jaccard, D.; Schneider, T.; Gabay, M.; Thiel, S.; Hammerl, G.; Mannhart, J.; Triscone, J. M. Electric Field Control of the $LaAlO_3/SrTiO_3$ Interface Ground State. *Nature* **2008**, *456*, 624−627.
(34) Bell, C.; Harashima, S.; Kozuka, Y.; Kim, M.; Kim, B. G.; Hikita, Y.; Hwang, H. Y. Dominant Mobility Modulation by the Electric Field Effect at the $LaAlO_3/SrTiO_3$ Interface. *Phys. Rev. Lett.* **2009**, *103*, 226802.
(35) Hosoda, M.; Hikita, Y.; Hwang, H. Y.; Bell, C. Transistor Operation and Mobility Enhancement in Top-Gated $LaAlO_3/SrTiO_3$ Heterostructures. *Appl. Phys. Lett.* **2013**, *103*, 103507.
(36) Eerkes, P. D.; van der Wiel, W. G.; Hilgenkamp, H. Modulation of Conductance and Superconductivity by Top-Gating in $LaAlO_3/SrTiO_3$ 2-Dimensional Electron Systems. *Appl. Phys. Lett.* **2013**, *103*, 201603.
(37) Forg, B.; Richter, C.; Mannhart, J. Field-Effect Devices Utilizing $LaAlO_3$-$SrTiO_3$ Interfaces. *Appl. Phys. Lett.* **2012**, *100*, 053506.
(38) Liu, W.; Gariglio, S.; Fete, A.; Li, D.; Boselli, M.; Stornaiuolo, D.; Triscone, J. M. Magneto-Transport Study of Top- and Back-Gated $LaAlO_3/SrTiO_3$ Heterostructures. *APL Mater.* **2015**, *3*, 062805.
(39) Cen, C.; Thiel, S.; Hammerl, G.; Schneider, C. W.; Andersen, K. E.; Hellberg, C. S.; Mannhart, J.; Levy, J. Nanoscale Control of an Interfacial Metal-Insulator Transition at Room Temperature. *Nat. Mater.* **2008**, *7*, 298−302.
(40) Tra, V. T.; Chen, J. W.; Huang, P. C.; Huang, B. C.; Cao, Y.; Yeh, C. H.; Liu, H. J.; Eliseev, E. A.; Morozovska, A. N.; Lin, J. Y.; Chen, Y. C.; Chu, M. W.; Chiu, P. W.; Chiu, Y. P.; Chen, L. Q.; Wu, C. L.; Chu, Y. H. Ferroelectric Control of the Conduction at the $LaAlO_3/SrTiO_3$ Heterointerface. *Adv. Mater.* **2013**, *25*, 3357−3364.
(41) Kim, S. I.; Kim, D. H.; Kim, Y.; Moon, S. Y.; Kang, M. G.; Choi, J. K.; Jang, H. W.; Kim, S. K.; Choi, J. W.; Yoon, S. J.; Chang, H. J.; Kang, C. Y.; Lee, S.; Hong, S. H.; Kim, J. S.; Baek, S. H. Non-Volatile Control of 2DEG Conductivity at Oxide Interfaces. *Adv. Mater.* **2013**, *25*, 4612−4617.
(42) Hurand, S.; Jouan, A.; Feuillet-Palma, C.; Singh, G.; Biscaras, J.; Lesne, E.; Reyren, N.; Barthelemy, A.; Bibes, M.; Villegas, J. E.; Ulysse, C.; Lafosse, X.; Pannetier-Lecoeur, M.; Caprara, S.; Grilli, M.; Lesueur, J.; Bergeal, N. Field-Effect Control of Superconductivity and Rashba Spin-Orbit Coupling in Top-Gated $LaAlO_3/SrTiO_3$ Devices. *Sci. Rep.* **2015**, *5*, 12751.
(43) Lin, W. N.; Ding, J. F.; Wu, S. X.; Li, Y. F.; Lourembam, J.; Shannigrahi, S.; Wang, S. J.; Wu, T. Electrostatic Modulation of $LaAlO_3/SrTiO_3$ Interface Transport in an Electric Double-Layer Transistor. *Adv. Mater. Interfaces* **2014**, *1*, 1300001.
(44) Xie, Y. W.; Hikita, Y.; Bell, C.; Hwang, H. Y. Control of Electronic Conduction at an Oxide Heterointerface Using Surface Polar Adsorbates. *Nat. Commun.* **2011**, *2*, 494.
(45) Au, K.; Li, D. F.; Chan, N. Y.; Dai, J. Y. Polar Liquid Molecule Induced Transport Property Modulation at $LaAlO_3/SrTiO_3$ Heterointerface. *Adv. Mater.* **2012**, *24*, 2598−2602.
(46) Ueno, K.; Shimotani, H.; Iwasa, Y.; Kawasaki, M. Electrostatic Charge Accumulation versus Electrochemical Doping in $SrTiO_3$ Electric Double Layer Transistors. *Appl. Phys. Lett.* **2010**, *96*, 252107.

DOI: 10.1021/acsnano.6b00409
ACS Nano 2016, 10, 4532−4537